New proposal to JLab PAC 27 December 3, 2004

Structure of the Roper resonance from measurements of the double-polarization $\mathbf{p}(\vec{e},e'\vec{p})\pi^0$ reaction

W. Bertozzi, O. Gayou (co-spokesperson), S. Gilad (co-spokesperson), P. Monaghan, A. Puckett, Y. Qiang, A. Shinozaki, Y. Xiao, X. Zhan, C. Zhang
Lab for Nuclear Science, Massachusetts Institute of Technology, Cambridge, MA

M. Potokar, S. Širca[1] (co-spokesperson)
J. Stefan Institute and Dept. of Physics, University of Ljubljana, Slovenia

A. Sarty (co-spokesperson)
Dept. of Astronomy and Physics, St. Mary's University, Halifax, Nova Scotia, Canada

Z.-L. Zhou
Schlumberger-Doll Research, Ridgefield, CT

V. Punjabi
Norfolk State University, Norfolk, VA

R. Roché
Old Dominion University, Norfolk, VA

D. W. Higinbotham
Thomas Jefferson National Accelerator Facility, Newport News, VA

C. F. Perdrisat
College of William and Mary, Williamsburg, VA

S. Strauch
The George Washington University, Washington, DC

P. Markowitz
Florida International University, Miami, FL

R. Gilman, R. D. Ransome
Physics Dept., Rutgers University, Piscataway, NJ

J. Calarco
University of New Hampshire, Durham, NH

L. Tiator, S. Kamalov
Institut für Kernphysik, University of Mainz, Germany and JINR, Dubna, Russia

[1]contact person, e-mail: sirca@jlab.org

Abstract

We propose to study the structure of the Roper resonance by a measurement of recoil proton polarization components in the $p(\vec{e}, e'\vec{p})\pi^0$ reaction in Hall A. The components exhibit strong sensitivities to the pertinent resonant Roper multipoles M_{1-} and S_{1-}, and will be measured in a broad range of Q^2 and W. The large kinematic coverage will allow us to attain a better overall understanding of the N → R transition amplitudes, for which only scarce data exist. These measurements will provide critical insight for extracting information on the N → R transition through comparison with the state-of-the-art models, and will also provide severe constraints on these models in the second resonance region.

The experiment requires 2 GeV and 3 GeV beams and the standard hardware configuration of Hall A. We request 348 hours of beam time.

Contents

1 Introduction

The $P_{11}(1440)$ (Roper) resonance [1] is the lowest positive-parity $N^\star$ state. It is visible in partial-wave decompositions of $\pi N \to \pi N$ and $\pi N \to \pi\pi N$ scattering [2, 3] as a shoulder around 1440 MeV with a width of about 350 MeV [4]. Its large width causes it to merge with the adjacent $D_{13}(1520)$ and $S_{11}(1535)$ resonances, and therefore it can not be resolved from the W-dependence of the cross-section alone. Although this four-star resonance is within the energy range of many modern facilities, the experimental analyses so far have not ventured far beyond the determination of its mass, widths, and photon decay amplitudes. Very little is known about its internal structure.

The purpose of this experiment is to study the structure of the Roper resonance by measuring the recoil proton polarization components P'_x, P_y, and P'_z in the $p(\vec{e}, e'\vec{p})\pi^0$ reaction over an extended range in Q^2 and W. In particular, the P'_x and P_y exhibit strong sensitivities to the resonant multipoles M_{1-} and S_{1-} relevant to Roper electro-production. The large kinematic coverage of our measurements will provide vital input the state-of-the-art models of pion electro-production in the second resonance region. It is for the first time that the Roper resonance is being approached by means of the recoil-polarization technique, although this strategy benefits substantially from the experience gained in the well-studied $N \to \Delta$ transition.

2 Physics overview and motivation

At present, only two models exist that are capable of computing full electro-production matrix elements with complex multipole structures. These models, and their connection to our measurement will be discussed in more detail in Subsection 2.2. On the other hand, numerous models have been developed to investigate the structure of the Roper resonance by studying the photo- and electro-excitation part of the process. These developments are summarized below.

In the simplest spherically symmetric quark model with SU(6) spin-flavour symmetry, the Roper resonance can be understood as a radial excitation of the proton, with one quark occupying the 2s state, yielding a $(1s)^2(2s)^1$ configuration. The spin, isospin and parity are assumed not to change in this transition, and hence the excitation can be viewed as a "breathing mode" of the proton. This physical picture implies a sizable Coulomb monopole contribution (C0 or S_{1-}) along with the only other allowed multipole, the magnetic dipole (M1 or M_{1-}).

Recent models [5, 6] have indicated a possible description of the Roper resonance as a gluonic partner of the proton, represented as a (q^3g) hybrid baryon. Hybrid baryons are states presumably dominated by the state of three quarks oscillating against explicitly excited configurations of the gluon fields. The energies of these excitations could be as low as 550 MeV, so the Roper state is a natural candidate. The problem is that the hybrid states may have the same quantum numbers as the three-quark states, thus

by spectroscopy alone, they are indistinguishable. However, hybrid and three-quark representations can be discriminated by virtue of different structures of the spatial and spin-flavour wave-functions. In hybrids, the radial wave-functions of the proton and the Roper are the same, while the spin-isospin parts are orthogonal. Since the radial wave-functions are equal, the matrix element of the charge operator vanishes (to lowest relativistic order). The C0 strength should thus be highly suppressed, implying a predominantly magnetic dipole transition, in contrast to the concept of "breathing".

These two opposing concepts result in rather different predictions for the Q^2-dependence of the transverse ($A^p_{1/2}$) and scalar ($S^p_{1/2}$) electro-production helicity amplitudes shown in Fig. 1. In the charged channel, the radially excited (q^3) state is predicted to have a characteristically slow fall-off of $A^p_{1/2}$ and $S^p_{1/2}$ which seems to be excluded by the scarce data. The predicted Q^2-dependence of $A^p_{1/2}$ for the hybrid (q^3g) state has a fall-off similar to the one seen in the N → Δ transition, while $S^p_{1/2}$ is predicted to be zero. The experimental photo-production data in the figure is from the PDG review [4], and both approaches mentioned above fail to reproduce these electromagnetic couplings.

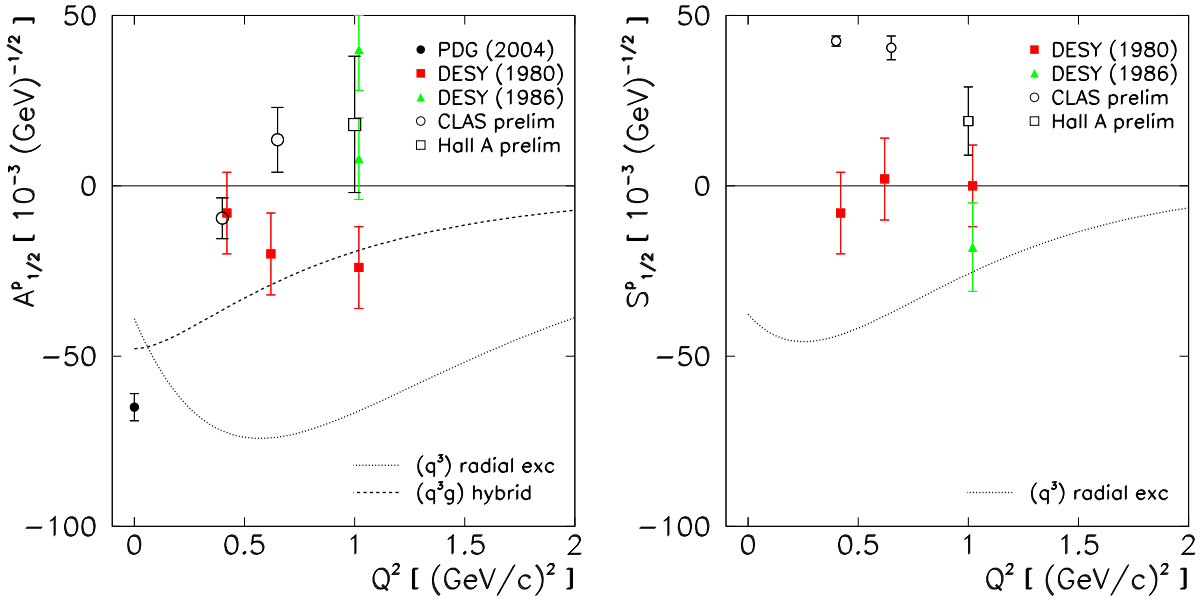

Fig. 1 — Nucleon-Roper transverse (left) and scalar (right) helicity amplitudes for the charged (proton) state. Published experimental data are from [4] for the photon point and from analyses [7, 8] of old unpolarized electro-production data for $Q^2 > 0$. The preliminary CLAS and Hall A data are discussed in Section 2.1. The curves are for a Roper as a radially excited (q^3) state or a (q^3g) hybrid state [6].

Experimentally, the Q^2-dependence of the helicity amplitudes is poorly known. A re-analysis of relatively old DESY and NINA electro-production experiments yielded $S^p_{1/2}$ consistent with zero, and gave contradictory results for the $A^p_{1/2}$. The lack of (double)-polarized measurements is, to a great extent, responsible for such large uncertainties. Newer polarized experiments at JLab (see below for details) have yielded more precise values of $S^p_{1/2}$ at $Q^2 = 0.4$ and $0.65\,(\mathrm{GeV/c})^2$. The $A^p_{1/2}$ has also been extracted at $Q^2 = 0.4$, 0.65, and $1.0\,(\mathrm{GeV/c})^2$. It appears to exhibit a zero-crossing in the vicinity of

$Q^2 = 0.5\,(\mathrm{GeV/c})^2$, although the situation remains unclear due to limited Q^2-coverage and modest error-bars (except for two points for $S^{\mathrm{p}}_{1/2}$).

The view of the Roper as a hybrid baryon has not been limited to the methods mentioned above. The Roper has also been investigated as a hybrid by using QCD sum rules [9] and in the domain of perturbative QCD [10]. The latter prediction, which can not be checked with the kinematic range of Hall A, states that if Roper is a hybrid, its electro-production rate should remain small asymptotically, whereas if it is a (q^3) state, it should not. In the most modern hybrid calculations [11, 12, 13], the Roper masses are well understood in terms of vibrating flux-tubes between quarks, but extensions of the models to dynamical processes are still lacking. Perhaps, Lattice QCD is the tool which will help remove the numerous controversies surrounding the Roper. Although some doubt persist on the four-star rating of the Roper, which appears to be unusually broad in partial-wave analyses of πN scattering, it has recently been observed clearly and at the correct energy on the lattice in a very precise calculation with a pion mass as low as 180 MeV [14]. This has been achieved in a quenched calculation, leading to a conclusion that the Roper resonance is a (q^3) state. Other identifications of the resonance have been reported [15, 16], but dynamical processes involving the Roper remain future work.

Extensive studies of the nature of the Roper resonance in the framework of constituent, non-relativistic, and relativized quark models also exist. In [17], the Roper has been studied in a semi-relativistic constituent-quark model based on a linear confinement potential. The approach resulted in a good description of the Roper mass and width, but failed to reproduce the photo-couplings. A closer agreement with the experimental couplings has been achieved in a potential quark model where the relativistic electromagnetic interaction Hamiltonian has been treated consistently to $\mathcal{O}(v^2/\mathrm{c}^2)$ for the quarks [18]. This calculation suggested that QCD configuration-mixing effects are important. In particular, it was shown that mixing may have an increasingly large influence on helicity amplitudes for increasing Q^2. A further improvement has been advanced by [19, 20], in a quark model with relativistic corrections to the transition operator where only mixed (non-relativistic) wave-functions orthogonal to the ground states have been used. However, the photo-couplings for the Roper resonance remained in a disagreement with the data by roughly a factor of two. More recent quark-model calculations formulated on the light-front [21, 22, 23] have not improved this discrepancy significantly. In a non-relativistic quark model based on an extension of the Roper photo-production to $Q^2 > 0$ with exchange of vector-mesons [24], a rather good agreement with the experimental couplings has been obtained, but this result is difficult to verify due to the current overwhelming lack of electro-production data.

The photo- and electro-excitation of the Roper resonance has also been approached in quark models with meson degrees of freedom. A fair understanding of the photo-couplings has been obtained if meson-exchange currents between quarks were introduced [25]. Similarly, if the Roper is treated in a relativistic quark model as a three-quark core with an admixture of a pion-baryon configuration [26], the predicted photo-couplings are quite close to the data. In the framework of the chiral chromo-dielectric model [27] (see also [28]), the Roper resonance is described in terms of three valence

quarks coupled to a cloud of chiral mesons (σ and π) and to a chromo-dielectric field which dynamically confines the quarks. The quarks are in the $(1s)^3$ configuration for the nucleon and $(1s)^2(2s)^1$ for the Roper, and the physical Roper emerges from a self-consistent variation of the radial fields. One of the outstanding features of this model, with some ingredients of the quark-level linear σ-model, is a rather strong meson cloud which has gained in merit in recent studies of the N $\rightarrow \Delta$ transition.

The importance of the pion cloud is inherent also to all versions of the cloudy bag model (CBM). Photo-couplings for the Roper resonance in the CBM have been calculated [29] and were found to depend strongly on the strength of the pion cloud. The analysis of [30, 31] also used CBM input to study the πN-scattering phase-shifts in the Roper region by examining the resonance widths with and without inclusion of the Roper as a radial excitation (a bare three-quark state). The results seem to exclude such a state.

2.1 Relation to other experiments

Single-pion electro-production experiments in the $p(e,e'p)\pi^0$ and $p(e,e'n)\pi^+$ channels have been conducted in all three Halls at Jefferson Lab. In most of the cases, only cross-sections (angular distributions) were measured. Only a handful of single- and double-polarization measurements have been performed so far.

Jefferson Lab: Hall B (CLAS)

Kinematically most extensive data sets on single-pion electro-production in the nucleon resonance regions come from Hall B. Angular distributions and W-dependence of the electron beam asymmetry $\sigma_{LT'}$ have been measured for both channels in the $P_{33}(1232)$ region at $Q^2 = 0.4$ and 0.65 $(\mathrm{GeV/c})^2$ [32, 33].

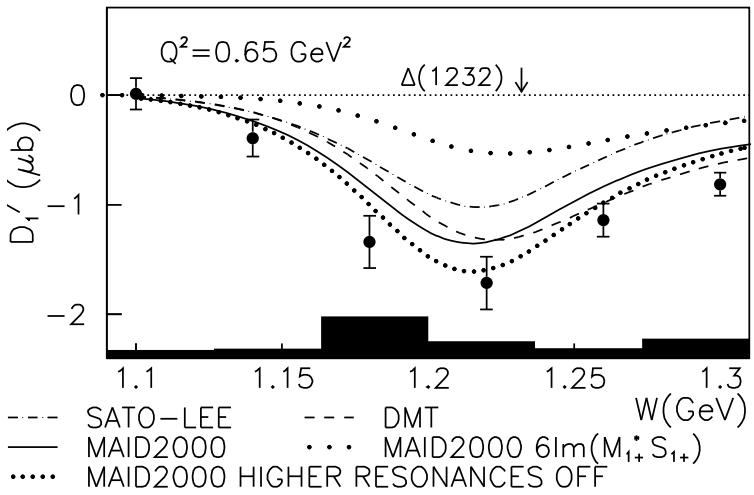

Fig. 2 — Comparison of model calculations to the CLAS measurement [32] of the first Legendre moment D_1' in the $p(e,e'p)\pi^0$ channel as a function of W.

A complete angular coverage was achieved, and different non-resonant amplitudes could be separated in a partial-wave analysis restricted to $l \leq 2$. The Legendre moments D'_0, D'_1, and D'_2 of the expansion

$$\sigma_{\mathrm{LT}'} = D'_0 + D'_1 P_1(\cos\theta^\star_\pi) + D'_2 P_2(\cos\theta^\star_\pi) + \cdots$$

were determined. The D'_1 moment (Fig. 2) appears to be the one most sensitive to higher resonances, with contributions of about $15-20\,\%$ coming mainly from the $\mathrm{Im}(M^*_{1-}S_{1+})$ interference, pointing to the relevance of the Roper.

Most recently, dispersion-relation techniques and unitary isobar models have been applied to analyze the CLAS $\sigma_{\mathrm{LT}'}$ data at $Q^2 = 0.4$ and $0.65\,(\mathrm{GeV/c})^2$ spanning also the second resonance region, in order to extract the contributions of the $P_{33}(1232)$, $P_{11}(1440)$, $D_{13}(1520)$, and $S_{11}(1535)$ resonances to single-pion production [34]. To achieve a successful fit of θ^*_π- and W-dependence of $\sigma_{\mathrm{LT}'}$ in terms of the usual pion-production models (MAID, Sato-Lee, and DMT), a simultaneous adjustment of the M_{1-} and S_{1-} amplitudes was needed. By using the JLab version of the unitary isobar model (JANR), which was shown to be consistent with the dispersion-relation approach, an excellent direct fit could be obtained. Since both the $\mathrm{p}\pi^0$ and the $\mathrm{n}\pi^+$ channel were measured (isospin), the transverse helicity amplitude $A^{\mathrm{p}}_{1/2} \propto_{\mathrm{p}} M^{1/2}_{1-}$ as well as the scalar $S^{\mathrm{p}}_{1/2} \propto_{\mathrm{p}} S^{1/2}_{1-}$ could be extracted. The results show a rapid fall-off of $A^{\mathrm{p}}_{1/2}$ and indicate its zero-crossing at $Q^2 \sim 0.5-0.6\,(\mathrm{GeV/c})^2$ (Fig. 1).

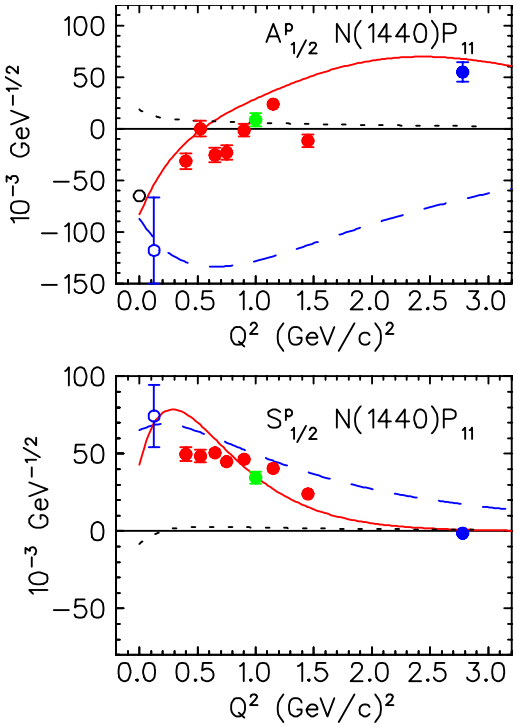

Fig. 3 — The Q^2-dependence of the P_{11} helicity amplitudes from the super-global solution of MAID 2003 (solid lines), based on data published prior to CLAS 2003 (see [35] for references to the input data sets). The dotted curves show *only* the pion-cloud contribution of the DMT model (see discussion in Subsection 2.2).

It was also shown that $\sigma_{LT'}$ is mainly sensitive to the imaginary part of $P_{11}(1440)$, while the cross-section is sensitive to the real part of P_{11} multipoles. A MAID 2003 super-global fit (Fig. 3, solid lines) to previously published $(e,e'p)\pi^0$ data also indicates a zero-crossing of $A^p_{1/2}$ at $Q^2 \sim 0.5\,(\mathrm{GeV/c})^2$, yet with a rather inconsistent systematic scatter of points representing single-Q^2 fits [35].

This (theoretical) uncertainty in locating the region in Q^2 in which both resonant Roper multipoles are substantial, was one of our motivations to investigate double-polarization observables sensitive to the structure of the Roper over a broader range in Q^2. In addition, a large lever-arm in W will allow us to approach the unknown behaviour of the transition amplitudes away from the resonance position (see below).

In Hall B, there is also an approved experiment E03-105 [36] that will measure single-pion photo-production in both $p(\gamma,\pi^+)n$ and $p(\gamma,p)\pi^0$ channels, with polarized beam and longitudinally as well as transversely polarized target using the CLAS detector. The experiment will measure two single- (T and P) and three double-polarization observables (G, F, and H); in addition, the experiment E01-104 will measure the double-polarization observable E. The measurements will span the energy range $1300 \le W \le 2150\,\mathrm{MeV}$ and achieve an angular coverage of $-0.9 \le \cos\theta^\star \le 0.9$. (In the Roper region, there is a competing real-photon experiment of the A2 Collaboration at Mainz measuring G, see below.)

It is believed that this data will greatly constrain partial-wave analyses in photo-production and reduce model-dependent uncertainties in the extraction of nucleon resonance properties. A similar goal, but in electro-production, and utilizing the recoil-polarimetry technique, is being pursued by our proposed experiment, and is thus to some extent complementary to the effort with CLAS.

Jefferson Lab: Hall A

Polarized electron beam and recoil-polarimetry capability of Hall A also allow access to double-polarization observables in single-pion electro-production. Recoil-polarization observables are composed of different combinations of multipole amplitudes than observables accessible in the case of a polarized target. In the sense of experimental method, the measurements proposed here are complementary to the efforts with CLAS in Hall B.

The acceptance of CLAS is large enough to achieve a complete angular coverage of the outgoing hadrons. This is not possible in the case of relatively small angular openings of the Hall A HRS spectrometers *except* at high Q^2 where the Lorentz boost from the center-of-mass to lab frame focuses the reaction products into a cone narrow enough to provide a virtually complete out-of-plane acceptance. The E91-011 experiment in Hall A in the $p(\vec{e},e'\vec{p})\pi^0$ channel [37] was performed at sufficiently high $Q^2 = (1.0 \pm 0.2)\,(\mathrm{GeV/c})^2$ and $W = (1.23 \pm 0.02)\,\mathrm{GeV}$ to allow for a measurement of all accessible response functions, even those that vanish for coplanar kinematics. Two Rosenbluth combinations and 14 structure functions could be separated, allowing for a restricted

partial-wave analysis giving access to all $l \leq 1$ multipole amplitudes relevant to the $N \rightarrow \Delta$ transition. The preliminary results for the M_{1-} and S_{1-} multipoles in the $p\pi^0$ channel are shown in Fig. 4. Both multipoles indicate a rising trend approaching the $W \sim 1440\,\text{MeV}$ region, again pointing towards the Roper.

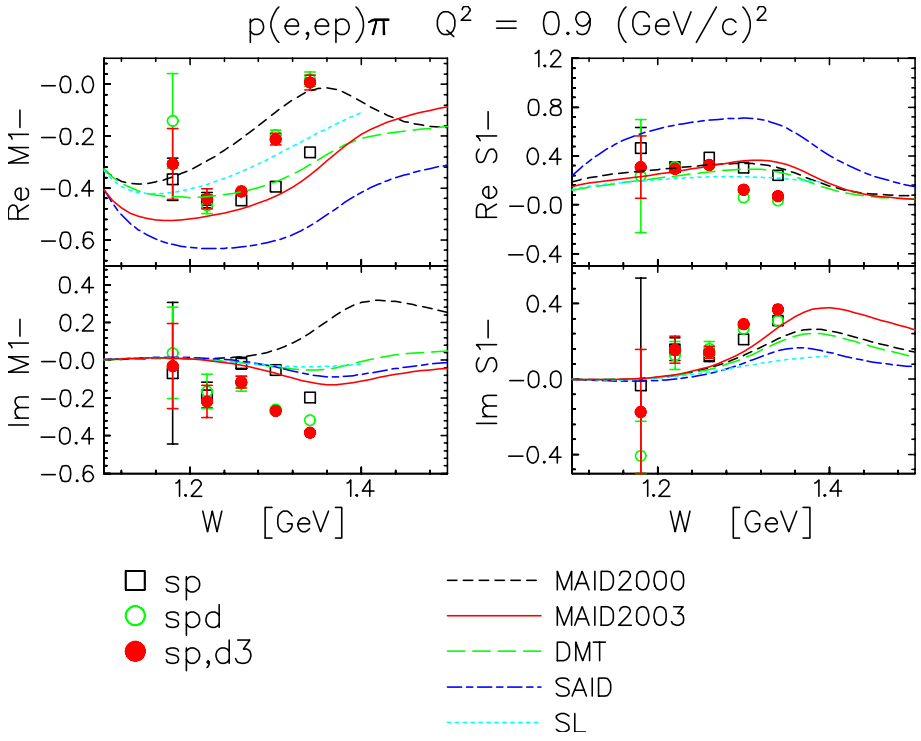

Fig. 4 — The W-dependence of the Re and Im parts of M_{1-} and S_{1-} multipoles in the $p(\vec{e}, e'\vec{p})\pi^0$ channel (preliminary results of the Hall A E91-011 experiment).

Unfortunately, the cross-sections at $W \sim 1440\,\text{MeV}$ (for any Q^2) are about an order of magnitude smaller than in the Δ-peak (see Fig. 5). For high $Q^2 \sim 1\,(\text{GeV/c})^2$, where a large out-of-plane coverage would allow for a decent partial-wave analysis in Hall A, the cross-sections are even smaller. Furthermore, due to the zero-crossing uncertainty of the M_{1-} multipole, it is not clear what value of Q^2 to choose in order to have a prominent $M1$ signal. Furthermore, models indicate that the crucial features of the Roper multipoles (or helicity amplitudes) are visible at relatively small Q^2 of a few $0.1\,(\text{GeV/c})^2$, nullifying the boost-advantage of the HRS.

We note in addition that higher partial waves ($l \geq 2$) in all JLab partial-wave analyses so far needed to be constrained by models (just as in the CLAS experiments). Thus, even with (almost) complete angular coverages, existing data sets of finite statistical certainty do not allow for a "full" partial-wave analysis to sufficiently large l.

Without a firmer guidance, and with the lack of instrumental advantage, we think that a measurement in the spirit of the E91-011, attempting a precise extraction of the Roper multipoles from a complete partial-wave analysis at a *single* Q^2-point, is not the most effective strategy at this moment. Instead, we believe that a precise measurement of a more restricted set of double-polarization observables, highly sensitive to the Roper

multipoles, and spanning a broad range in Q^2 and W, will yield a more rewarding and critical insight into the structure of the N → R transition through comparison with models. Further details are given in Sections 3 and 4.

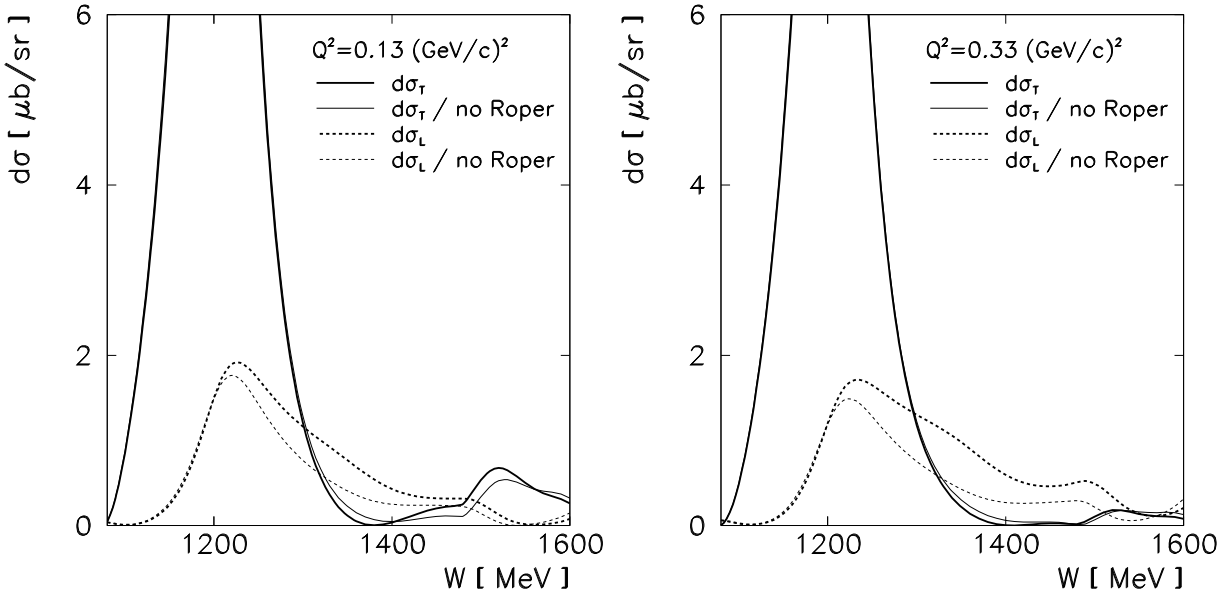

Fig. 5 — The W-dependence of the transverse and longitudinal CM cross-sections at $Q^2 = 0.1$ and 0.3 $(\mathrm{GeV/c})^2$, with the contribution of the Roper resonance on and off.

MAMI: A2

In photo-production, the double-polarization asymmetry G for linearly polarized photons (P_γ) and target nucleons polarized longitudinally (P_z) along the photon momentum, exhibits a very strong sensitivity to the Roper resonance. It is defined as

$$G = \frac{\mathrm{d}\sigma(\Phi = 45^\circ, z) - \mathrm{d}\sigma(\Phi = -45^\circ, z)}{\mathrm{d}\sigma(\Phi = 45^\circ, z) + \mathrm{d}\sigma(\Phi = -45^\circ, z)} ,$$

where Φ is the angle between the photon polarization plane and the reaction plane. The cross-section has the form

$$\mathrm{d}\sigma(\theta_\pi, \Phi) = \mathrm{d}\sigma(\theta_\pi)\Big(1 - P_\gamma \, \Sigma(\theta_\pi) \, \cos 2\Phi + P_\gamma P_z \, G(\theta_\pi) \, \sin 2\Phi \Big) .$$

In the $\vec{\gamma}\vec{\mathrm{p}} \to \mathrm{p}\pi^0$ reaction, G depends on the interference of the much better-known M_{1+} multipole governed by the $\Delta(1232)$, and the M_{1-} driven by the Roper,

$$G(\theta_\pi) \simeq \sin^2 \theta_\pi \; \mathrm{Im}M_{1+} \, \mathrm{Re}M_{1-} .$$

The asymmetry G will be measured by virtue of its $\sin 2\Phi$-dependence at the A2 Collaboration at MAMI with the Φ-symmetric detector DAPHNE. The expected sensitivity is shown in Fig. 6. In addition to the $\mathrm{p}\pi^0$, the $\mathrm{n}\pi^+$ channel will be measured, allowing for the isospin decomposition of the partial waves.

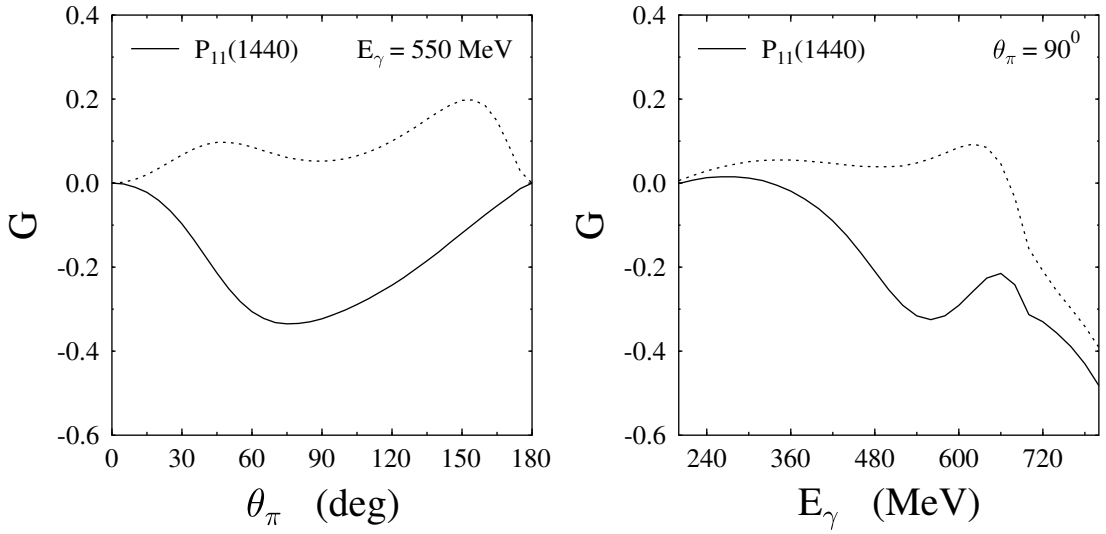

Fig. 6 — MAID prediction for G in the $\vec{y}\vec{p} \to p\pi^0$ reaction: angular distribution at $W = 1440\,\mathrm{MeV}$ and energy dependence at $\theta_\pi = 90°$. The dotted curves correspond to the Roper switched off.

MAMI: A1

All three recoil polarization components (P'_x/P_e, P_y, and P'_z/P_e) in the $p(\vec{e}, e'\vec{p})\pi^0$ reaction at the Δ resonance, at $Q^2 = 0.121\,(\mathrm{GeV/c})^2$ have been measured by the A1 Collaboration at MAMI [38] (see Fig. 7).

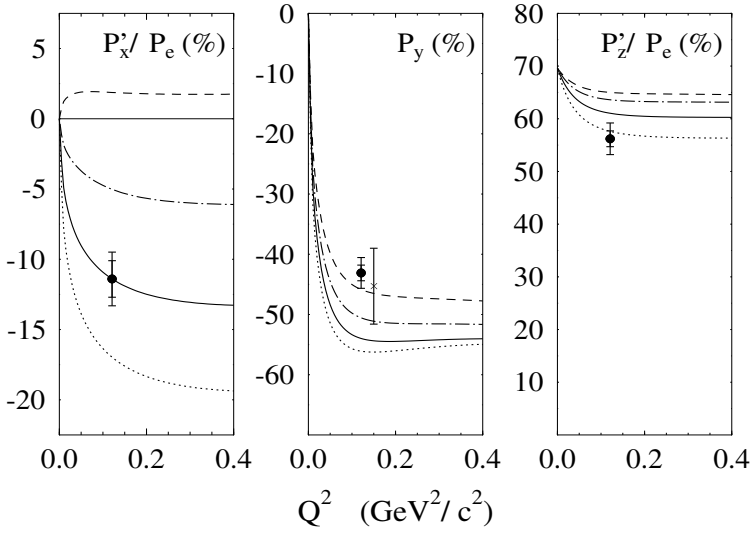

Fig. 7 — MAMI results for the recoil polarization components in $p(\vec{e}, e'\vec{p})\pi^0$ at $W = 1232\,\mathrm{MeV}$ and $Q^2 = 0.121\,(\mathrm{GeV/c})^2$, compared to MAID 2000 calculations. The dashed, dot-dashed, full, and dotted curves correspond to CMR = $\mathrm{Im}S_{1+}^{(3/2)}/\mathrm{Im}M_{1+}^{(3/2)}$ of 0 %, −3.2 %, −6.4 %, and −9.6 %, respectively.

These components, in particular the P'_x, were shown to be highly sensitive to the Coulomb quadrupole to magnetic dipole ratio CMR = $\mathrm{Im}S_{1+}^{(3/2)}/\mathrm{Im}M_{1+}^{(3/2)}$ in the N → Δ transition. Note, however, that the changes in the CMR (i.e. in the corresponding S_{1+} multipole) between the curves in Fig. 7 are quite large (±50 %).

Even this single-Q^2, single-W measurement for a "well-known" resonance warranted a publication in Phys. Rev. Lett. Our proposed measurement will extend this approach into the domain of the poorly-known Roper resonance, and will cover a much larger region in Q^2 and W.

Note that a straight-forward extension of the N → Δ program in the $\vec{\mathrm{p}}\pi^0$ channel into the Roper region appears to be impossible at Mainz/A1 due to instrumental constraints.

2.2 Relevance to pion electro-production models

The numerous models mentioned in the Introduction, although conceptually rich, are not in a stage at which they could be confronted with double-polarization observables with complex multipole structures, mostly because of an incomplete treatment of backgrounds, or due to an inability to include higher resonances. For a comprehensive description of resonance dynamics, three state-of-the-art pion electro-production models are available: the unitary isobar model MAID [39] and the dynamical models of the Dubna-Mainz-Taipei group (DMT) [40, 41] and Sato and Lee (SL) [42]. All these models were put to thorough verification when exposed to recent N → Δ transition double-polarization data from MIT-Bates, MAMI, and JLab, with varying success. Extrapolations into the Roper region remain a challenge for all, and two of them (MAID and DMT) can be directly tested with our proposed measurements.

Unitary isobar model (MAID)

The **MAID** model is based on effective Lagrangians with numerous adjustable parameters. The backgrounds are described by nucleon Born terms and vector-meson exchange terms, while the resonant contributions to each of the electro-production multipoles are parameterized by Breit-Wigner forms. The total amplitude is unitarized.

In MAID, the imaginary parts of the M_{1-} and S_{1-} multipoles for isospin $1/2$ are dominated by the resonant contributions. Therefore, the separation of the resonance from the background is relatively unproblematic for the Roper, the main challenge is a good determination of the multipoles themselves. A partial-wave analysis is therefore essential, and it can only be improved by measuring very sensitive observables that are used in the fits. In photo-production, high-quality data are available, and the multipole analyses over extended W-ranges result in good global fits. In electro-production, additional precise measurements of both cross-sections and (double-)polarization observables are badly needed in order to stabilize the fits.

Ideally, partial-wave analyses require complete data sets taken at particular values of Q^2. In reality, for example, CLAS has acquired "low-Q^2" data while Hall A covered a narrow range at "high Q^2". The MAID group therefore has recently been pursuing another direction by proposing "super-global" partial-wave analyses in which the Q^2-dependence of the multipoles is also parameterized by smooth functions. Such an analysis is then "fed" by practically all available photo- and electro-production data.

This approach is expected to work, and can even be refined, for smaller ranges in Q^2 and W. Following this guideline [46], we shall restrict the Q^2-coverage to the range $0 < Q^2 < 1\,(\mathrm{GeV/c})^2$, and span a controllable energy range ($\simeq 100\,\mathrm{MeV}$) in the vicinity of the resonance position. We depart intentionally, and with a purpose, from the well-established practice of measuring (only) at the resonance position: the energy dependence is badly needed for robust fits.

Dynamical models (DMT, SL)

The crucial feature of the dynamical (microscopic) approaches to pion electro-production is the inclusion of the final-state πN interaction such that the unitarity is preserved in the theory. In the **DMT model**, this is achieved by coupling the $\gamma^\star \mathrm{N} \to \pi\mathrm{N}$ transition potential to the πN t-matrix, where the transition potential consists of the background part and the bare resonance part.

In the following, we use the most recent versions of the DMT model (2001) and the MAID model (2003) in comparisons.

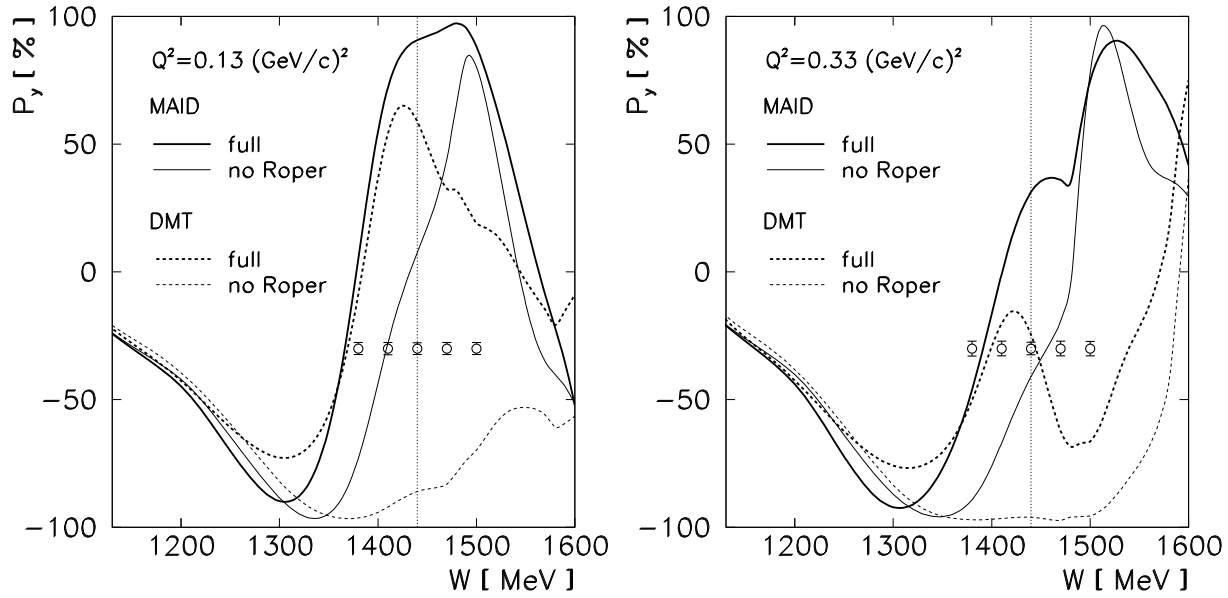

Fig. 8 — The MAID and DMT predictions for the W-dependence of P_n at $Q^2 = 0.13$ and $0.33\,(\mathrm{GeV/c})^2$, with the contribution of the Roper resonance on and off. The expected statistical uncertainty of our measurement is also shown.

While MAID and DMT agree on the cross-sections, they predict quite different Q^2- and W-dependences of recoil polarization amplitudes (in particular the P_y), and exhibit distinct sensitivities to the Roper multipoles (see Fig. 8). The variation in the sensitivities is due to the difference in the way resonances are treated in isobar models like MAID, compared to that in dynamical models like DMT. In isobar models, the EM vertices of resonances are "dressed" (i.e. they already contain pion-cloud contributions), so the resonance parameters in these models are directly comparable to the experimentally determined (PDG) values. In dynamical models, the resonances are "bare", and thus more consistent with e.g. quark-model predictions. The proposed measurement will be an important step towards drawing a distinction between the "dressed" and "bare" approaches (see also Fig. 3).

At present, the **SL model** is not applicable to the meson electro-production reactions above the delta resonance region. Attempts are being made to extend the model to higher energies, but the extension requires considerable effort. The authors do believe [45] that it is important to map the energy- and Q^2-dependence of the P_{11} amplitudes in constraining the nature of Roper resonance and dynamics in the 1.4 GeV region.

3 Formalism of the $\mathbf{p}(\vec{e}, e'\vec{p})\pi^0$ reaction

The cross-section for the $p(\vec{e}, e'\vec{p})\pi^0$, allowing for both a polarized electron beam and detection of the recoil proton polarization, is given by [47]

$$\frac{d\sigma}{dE'_e\, d\Omega_e\, d\Omega^\star_p} = \frac{\sigma_0}{2}\Big\{ 1 + \boldsymbol{P}\cdot\hat{\boldsymbol{s}}_r + h\Big[A_e + \boldsymbol{P}'\cdot\hat{\boldsymbol{s}}_r\Big]\Big\}, \tag{1}$$

where $\sigma_0 \equiv d\sigma(\hat{\boldsymbol{s}}_r) + d\sigma(-\hat{\boldsymbol{s}}_r)$ is the unpolarized cross-section, $\hat{\boldsymbol{s}}_r$ is the proton spin vector in its rest frame, h is the helicity of the incident electrons, $\boldsymbol{P}$ is the induced proton polarization, A_e is the beam analyzing power, and $\boldsymbol{P}'$ is the vector of spin-transfer coefficients. The polarization of the recoiled proton consists of a helicity-independent (induced) and a helicity-dependent (transferred) part, $\boldsymbol{\Pi} \equiv \boldsymbol{P} + h\boldsymbol{P}'$. The cross-section can be cast in a form in which the electron vertex is evaluated in the lab frame, while hadronic quantities are in the CM frame of the πN final state. In terms of response functions, the cross-section is

$$\begin{aligned}
\frac{d\sigma}{dE'_e\, d\Omega_e\, d\Omega^\star_p} = \Gamma_v \frac{|\boldsymbol{p}^\star_p|\, W}{K_y M_p} \Big\{ & (R_T + R^n_T S_n) + 2\varepsilon^\star_L (R_L + R^n_L S_n) \\
& + \sqrt{\varepsilon^\star_L(1+\varepsilon)}\Big[(R_{LT} + R^n_{LT} S_n)\cos\phi + (R^l_{LT} S_l + R^t_{LT} S_t)\sin\phi \Big] \\
& + \varepsilon \Big[(R_{TT} + R^n_{TT} S_n)\cos 2\phi + (R^l_{TT} S_l + R^t_{TT} S_t)\sin 2\phi \Big] \\
& + h\sqrt{\varepsilon^\star_L(1-\varepsilon)}\Big[(R'_{LT} + R'^n_{LT} S_n)\sin\phi + (R'^l_{LT} S_l + R'^t_{LT} S_t)\cos\phi \Big] \\
& + h\sqrt{1-\varepsilon^2}\Big[R'^l_{TT} S_l + R'^t_{TT} S_t \Big] \Big\},
\end{aligned} \tag{2}$$

where M_p is the proton mass, W is the invariant mass of the πN final state, Γ_v is the virtual photon flux, and $K_y = (W^2 - M_p^2)/2W$ is the equivalent real-photon energy.

The ε is the transverse polarization of the virtual photon. The subscripts T, L, LT, and TT denote transverse, longitudinal, longitudinal-transverse, and transverse-transverse interference terms, the primes denote those response functions which can only be accessed by using polarized electrons, and the * denotes CM quantities. The longitudinal polarization of the virtual photon is $\varepsilon_{\rm L}^\star \equiv \varepsilon(Q^2/|\boldsymbol{q}^\star|^2)$, and $S_{\rm n,l,t}$ are the projections of the proton spin vector, given by $S_{\rm t} = \hat{\boldsymbol{t}} \cdot \hat{\boldsymbol{s}}_{\rm r}$, $S_{\rm n} = \hat{\boldsymbol{n}} \cdot \hat{\boldsymbol{s}}_{\rm r}$, and $S_{\rm l} = \hat{\boldsymbol{l}} \cdot \hat{\boldsymbol{s}}_{\rm r}$. The projections are given in the coordinate frame of the reaction plane which is tilted at an angle of $\phi_{\rm pq}^\star \equiv \phi$ with respect to the electron scattering plane (see Fig. 9), $\hat{\boldsymbol{l}}$ is along proton momentum, $\hat{\boldsymbol{n}}$ is normal to the reaction plane, and $\hat{\boldsymbol{t}} = \hat{\boldsymbol{n}} \times \hat{\boldsymbol{l}}$.

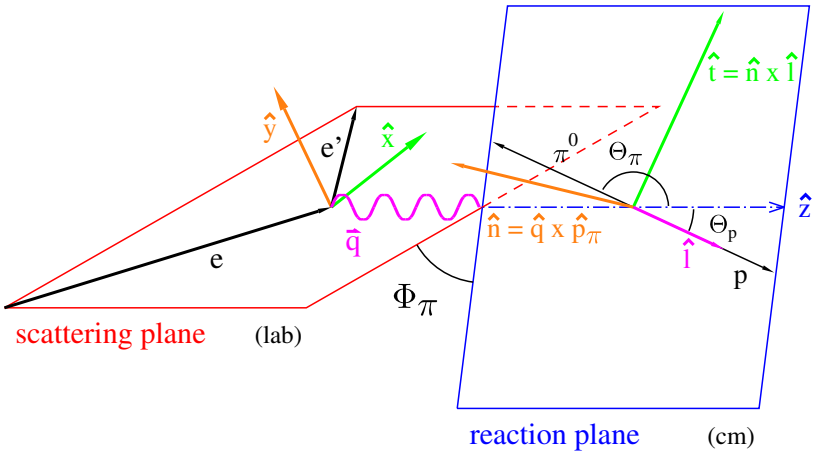

Fig. 9 — Schematic representation of the $\mathrm{p}(\vec{\mathrm{e}},\mathrm{e}'\vec{\mathrm{p}})\pi^0$ reaction.

For measurements in the (e,e') scattering plane, the polarization components $\boldsymbol{\Pi}$ can be extracted by comparing coefficients in (1) and (2) and by using $\boldsymbol{\Pi} \cdot \hat{\boldsymbol{s}}_{\rm r} = \Pi_{\rm t} S_{\rm t} + \Pi_{\rm n} S_{\rm n} + \Pi_{\rm l} S_{\rm l}$,

$$
\begin{aligned}
\tilde{\sigma}_0 \Pi_{\rm t} &= h\Big[\sqrt{1-\varepsilon^2}\, R_{\rm TT}^{\prime\rm t} \pm \sqrt{\varepsilon_{\rm L}^\star(1-\varepsilon)}\, R_{\rm LT}^{\prime\rm t}\Big]\,, \\
\tilde{\sigma}_0 \Pi_{\rm n} &= R_{\rm T}^{\rm n} + 2\varepsilon_{\rm L}^\star R_{\rm L}^{\rm n} \pm \sqrt{\varepsilon_{\rm L}^\star(1+\varepsilon)}\, R_{\rm LT}^{\rm n} + \varepsilon\, R_{\rm TT}^{\rm n}\,, \\
\tilde{\sigma}_0 \Pi_{\rm l} &= h\Big[\sqrt{1-\varepsilon^2}\, R_{\rm TT}^{\prime\rm l} \pm \sqrt{\varepsilon_{\rm L}^\star(1-\varepsilon)}\, R_{\rm LT}^{\prime\rm l}\Big]\,,
\end{aligned}
$$

where $\tilde{\sigma}_0$ is the unpolarized cross-section, except for a term proportional to $\sigma_{\rm Mott}$,

$$
\tilde{\sigma}_0 = R_{\rm T} + 2\varepsilon_{\rm L}^\star R_{\rm L} \pm \sqrt{\varepsilon_{\rm L}^\star(1+\varepsilon)}\, R_{\rm LT} + \varepsilon\, R_{\rm TT}\,,
$$

and the $\pm$ signs correspond to $\phi = 0^\circ$ and 180°, respectively. In the case of parallel kinematics with $\boldsymbol{q} \parallel \boldsymbol{p}_{\rm p}$, the components of the proton polarization reduce to

$$
\begin{aligned}
\tilde{\sigma}_0 \Pi_{\rm t} &= h\sqrt{\varepsilon_{\rm L}^\star(1-\varepsilon)}\, R_{\rm LT}^{\prime\rm t}\,, \\
\tilde{\sigma}_0 \Pi_{\rm n} &= \sqrt{\varepsilon_{\rm L}^\star(1+\varepsilon)}\, R_{\rm LT}^{\rm n}\,, \text{ and} \\
\tilde{\sigma}_0 \Pi_{\rm l} &= h\sqrt{1-\varepsilon^2}\, R_{\rm TT}^{\prime\rm l}
\end{aligned}
$$

due to an explicit $\sin\theta_{\rm pq}^\star$-dependence of some response functions. In parallel kinematics, the components of the polarization transverse to the proton momentum can

be arbitrarily defined, and it is convenient to choose the polarization reference frame such that P'_x (or P_t) is the one component unaffected by the precession in the spectrometers (parallel to the magnetic field), P'_z (or P_l) is along the central ray, while P_y (or P_n) is the "normal" component. We will use the (x', y, z') notation in the following.

The recoil proton polarization components in parallel (or anti-parallel) kinematics for the *pion* (i.e. $\cos\theta = \pm 1$) can be expressed in terms of three structure functions:

$$\sigma_0(P'_x/P_e) = \pm\sqrt{2\varepsilon_L^\star(1-\varepsilon)}\, R^t_{LT'}\,, \tag{3}$$

$$\sigma_0 P_y = -\sqrt{2\varepsilon_L^\star(1+\varepsilon)}\, R^n_{LT}\,, \tag{4}$$

$$\sigma_0(P'_z/P_e) = \mp\sqrt{1-\varepsilon^2}\, R^l_{TT'}\,. \tag{5}$$

where P_e is the electron polarization. The multipole decomposition of $R^t_{LT'}$ up to p-waves is

$$\begin{aligned} R^t_{LT'} = \mathrm{Re}\{\, & L^*_{0+}(2M_{1+}+M_{1-}) + (2L^*_{1+}-L^*_{1-})E_{0+} \\ & -\cos\theta\,(\, L^*_{0+}E_{0+} - 2L^*_{1+}(3E_{1+}+7M_{1+}+2M_{1-}) + L^*_{1-}(3E_{1+}+7M_{1+}+2M_{1-})\,) \\ & -\cos^2\theta\,(\, 3L^*_{0+}(E_{1+}+M_{1+}) + 6L^*_{1+}E_{0+}\,) \\ & -\cos^3\theta\,(\, 18L^*_{1+}(E_{1+}+M_{1+})\,)\,\} \end{aligned} \tag{6}$$

(note that the scalar and longitudinal multipoles are connected through $L \equiv (\omega/q)S$). In anti-parallel kinematics, the $R^t_{LT'}$ and R^n_{LT} measure the real and the imaginary parts respectively of the same combination of interference terms given by (6), up to a sign:

$$\begin{aligned} P'_x \sim R^t_{LT'} = \mathrm{Re}\{\, & L^*_{0+}E_{0+} \\ & +(L^*_{0+}-4L^*_{1+}-L^*_{1-})M_{1-} \\ & +L^*_{1-}(M_{1+}-E_{0+}+3E_{1+}) \\ & -L^*_{0+}(3E_{1+}+M_{1+}) + L^*_{1+}(4M_{1+}-E_{0+}) + 12L^*_{1+}E_{1+}\,, \end{aligned} \tag{7}$$

$$P_y \sim R^n_{LT} = -\,\mathrm{Im}\{\cdots\}\,. \tag{8}$$

In the case of the Roper resonance, the "$M1$-dominance" approximation applicable in the Δ region can not be used as many multipoles are comparable in size. With model guidance (MAID), we can estimate the role of individual terms in the expansion. The $L^*_{0+}E_{0+}$ interference is relatively large and prominent in all kinematics. The combinations $L^*_{1-}(-E_{0+}+3E_{1+})$ and $(-4L^*_{1+}-L^*_{1-})M_{1-}$ involving M_{1-} and/or L_{1-} are either relatively small or cancel substantially. The terms largest in magnitude and sensitivity are the $L^*_{0+}M_{1-}$ and the $L^*_{1-}M_{1+}$ each involving one of the relevant Roper multipoles linearly. It will be shown in Section 4 that the contributions of the M_{1-} and S_{1-} multipoles to P'_x and P_y depend strongly on Q^2 and W, so a measurement of P'_x and P_y in a broad range of Q^2 and W will allow us to quantify these dependencies.

The expansion of the $R^l_{TT'}$ response (or P'_z) in anti-parallel kinematics is

$$\begin{aligned} P'_z \sim R^l_{TT'} = \mathrm{Re}\{\, & E^*_{0+}(3E_{1+}+M_{1+}+2M_{1-})\,\} \\ & +|E_{0+}|^2 + 9\,|E_{1+}|^2 + |M_{1+}|^2 + |M_{1-}|^2 \\ & -6\,\mathrm{Re}E^*_{1+}M_{1+} - 2\,\mathrm{Re}M^*_{1+}M_{1-} - 3\,\mathrm{Re}E^*_{0+}(3E_{1+}+M_{1+})\,. \end{aligned}$$

This response is dominated by E_{0+} and M_{1+} multipoles and is therefore less sensitive to the Roper, but it is still important as a benchmark measurement and for calibration purposes. Most of our attention will be devoted to P'_x and P_y.

4 Proposed measurement

We believe that an attempt at a large-scale analysis of the Roper multipoles, aiming at a complete partial-wave analysis at a single Q^2-point in the spirit of the N → Δ experiment E91-011 [37], is at present not the most effective approach to study the structure of the N → R transition. Following the strategy outlined above, we propose a precise measurement of recoil polarization components which exhibit high sensitivities to the Roper resonant multipoles and span a broad range in Q^2 and W. It is this extended coverage that will allow for a more instructive study of the transition through comparison with models.

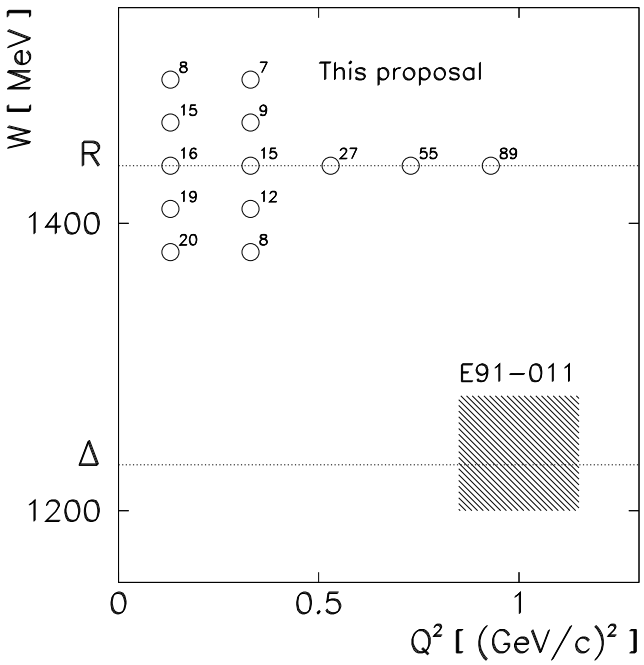

Fig. 10 — The kinematic coverage in W and Q^2 of the E91–011 experiment in Hall A (hatched area) and of the present proposal. The requested beam-hours per kinematic point are given next to the symbols (discussed below).

We will perform two W-scans at fixed Q^2 of 0.13 and 0.33 $(\mathrm{GeV/c})^2$ to explore the behaviour on and away from the resonance position, and a more extensive Q^2-scan at the resonance position $W = 1440\,\mathrm{MeV}$, with two overlapping settings. The W-scans will be performed at relatively small Q^2 because the predicted asymmetries and their sensitivities to the relevant multipoles appear to be largest there. Two beam energies (2 and 3 GeV) will be used. The lower beam energy is needed in order to accomodate the low-Q^2 end of the Q^2-scan (and the corresponding W-scan) without running into

the geometrical limits of the HRS spectrometers in Hall A. The proposed kinematics coverage is illustrated in Fig. 10 and listed explicitly in Table 1.

Table 1 — Proposed kinematics for the beam energies of 2000 and 3000 MeV (the $\star$ and $\star\star$ symbols denote duplicate entries measured only once). For a graphic representation of the (W, Q^2)-coverage, see Fig. 10.

E_e [MeV]	Q^2 [(GeV/c)^2]	W [MeV]	ε	E'_e [MeV]	θ_e [°]	p_p [MeV/c]	θ_p [°]
*2000	0.13	1440	0.8908	1294.9	12.9	1015	21.3
**3000	0.33	1440	0.9291	2188.3	12.9	1188	29.4
3000	0.53	1440	0.8990	2081.7	16.8	1343	30.8
3000	0.73	1440	0.8658	1975.1	20.2	1487	30.8
3000	0.93	1440	0.8294	1868.5	23.5	1625	30.1
2000	0.13	1380	0.9151	1385.0	12.4	914	24.7
2000	0.13	1410	0.9036	1340.4	12.6	964	23.0
*2000	0.13	1440	0.8908	1294.9	12.9	1015	21.3
2000	0.13	1470	0.8764	1248.3	13.1	1066	19.8
2000	0.13	1500	0.8604	1200.8	13.4	1118	18.5
3000	0.33	1380	0.9407	2278.4	12.6	1094	32.7
3000	0.33	1410	0.9352	2233.8	12.7	1140	31.0
**3000	0.33	1440	0.9291	2188.3	12.9	1188	29.4
3000	0.33	1470	0.9224	2141.7	13.0	1236	27.8
3000	0.33	1500	0.9151	2094.3	13.2	1285	26.4

4.1 Measurements at fixed Q^2 ("W-scans") vs. fixed W ("Q^2-scans")

The sensitivity of P_y to the resonant Roper multipoles M_{1-} (proportional to the helicity coupling $A^p_{1/2}$) and S_{1-} (proportional to $S^p_{1/2}$) is different at low and high Q^2, and varies through the W-range. At $Q^2 = 0.13\,(\mathrm{GeV/c})^2$ (Fig. 11 left), the full prediction for P_y at the resonance position is almost +100 %, with comparable M_{1-} and S_{1-} contributions, while it is close to zero with the Roper switched off. At $Q^2 = 0.33\,(\mathrm{GeV/c})^2$, P_y drops to about +40 % (Fig. 11 right), dropping to about −40 % with the Roper switched off, with different roles of M_{1-} and S_{1-}. At high $Q^2 = 0.73\,(\mathrm{GeV/c})^2$ and above (not shown), the full P_y is about −50 %, and only S_{1-} plays an appreciable role.

The role of the resonant multipoles changes very quickly, resulting in dramatic changes in the polarization components on a relatively narrow range in W (about ±60 MeV away from the resonance position to each side plus some additional coverage due to extended acceptance). The P_y being so large (on the order of several tens of %), a measurement in a broad range of Q^2 and W will therefore allow us to study its de-

pendencies quite precisely. The P'_x component bears similar sensitivities and is shown together with P'_z at $Q^2 = 0.13\,(\mathrm{GeV/c})^2$ in Fig. 12.

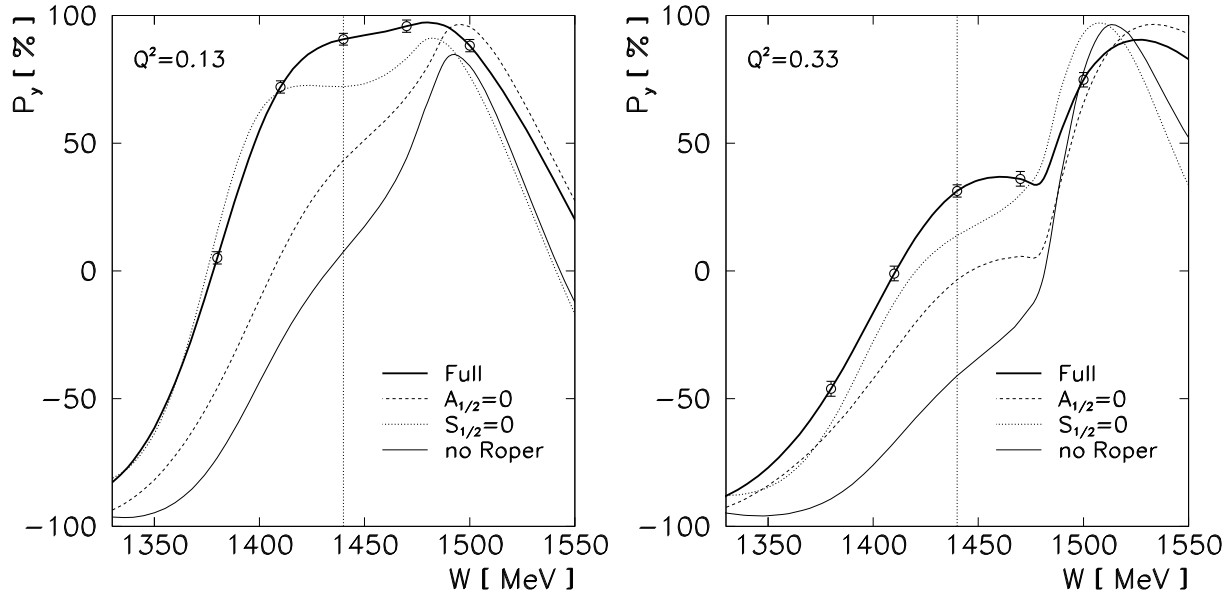

Fig. 11 — Sensitivity of P_y to the resonant Roper multipoles M_{1-} (helicity amplitude $A^{\mathrm{p}}_{1/2}$) and S_{1-} ($S^{\mathrm{p}}_{1/2}$), as a function of W at $Q^2 = 0.13$ and $0.33\,(\mathrm{GeV/c})^2$. The expected statistical uncertainties of the proposed measurement are also shown.

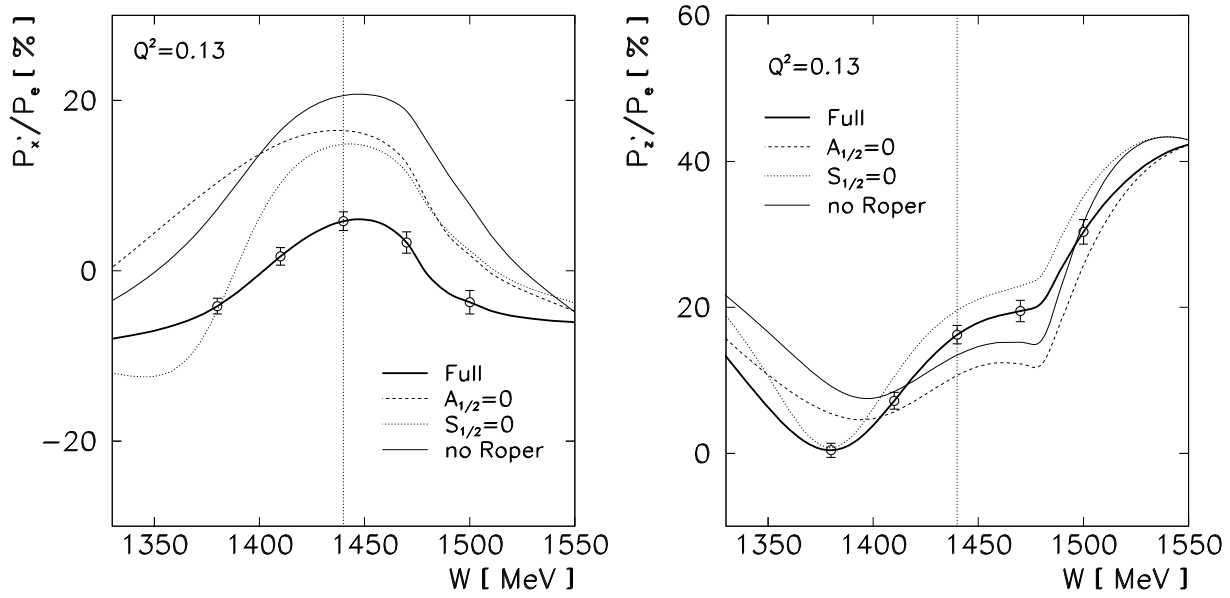

Fig. 12 — Sensitivity of P'_x/P_{e} and P'_z/P_{e} to the resonant Roper multipoles M_{1-} (helicity amplitude $A^{\mathrm{p}}_{1/2}$) and S_{1-} ($S^{\mathrm{p}}_{1/2}$), as a function of W at $Q^2 = 0.13\,(\mathrm{GeV/c})^2$. The expected statistical uncertainties of the proposed measurement are also shown. Note the change of scales.

The W-dependencies of both P'_x and P'_z become washed out at high Q^2. However, the large asymmetries persist in P_y and, to some extent, also in the P'_x. A measurement of the Q^2-dependence of P_y and P'_x (see Fig. 13) therefore gives us yet another handle to quantify the role of the individual multipoles, and can be mapped onto the zero-crossing of the $A^p_{1/2}$ helicity amplitude (see e.g. Fig. 3). As it has been discussed above, this additional lever-arm is of crucial importance for partial-wave analyses.

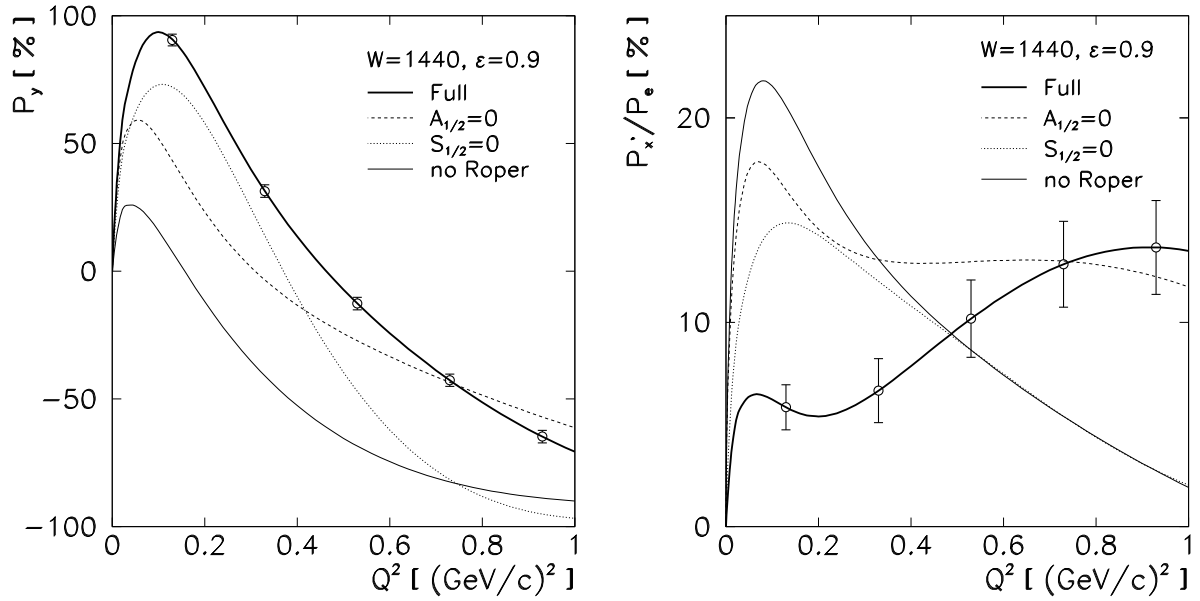

Fig. 13 — Sensitivity of the normal (induced) recoil polarization component P_y and of the in-plane component P'_x/P_e to the resonant Roper multipoles M_{1-} (helicity amplitude $A^p_{1/2}$) and S_{1-} ($S^p_{1/2}$), as a function of Q^2 at $W = 1440$ MeV. The expected statistical uncertainties of the proposed measurement are also shown. Since the virtual photon polarization ε differs slightly over the given Q^2-range, the plots were generated with an average $\varepsilon \simeq 0.9$.

5 Experimental equipment and methods

5.1 Focal-plane polarimeter

The ejected proton polarization will be measured by the focal plane polarimeter (FPP), located in the right-arm High-Resolution Spectrometer (HRS) of Hall A. This polarimeter has been used in numerous Jefferson Lab experiments, and its operation presents no difficulty.

It consists of four blocks of graphite analyzer ("carbon doors") of different thicknesses (1.5", 3", 6" and 9") that can be opened or closed independently (in or out of the proton's way) to allow for many different possible thicknesses ranging from 3.81 cm to 49.58 cm, to optimize the efficiency. The protons undergo a scattering in the analyzer, and asymmetries in the azimuthal angular distribution of this scattering are propor-

tional to the two components of the polarization that are perpendicular to the momentum. The scattering angle is measured by detecting the incoming and outgoing tracks in two sets of straw chambers. The size and position of the rear chambers are optimized so that the geometrical efficiency for protons with scattering angle up to 20° is almost 100%.

The azimuthal angular distribution of the scattering in the analyzer is given by

$$N^{\pm}(\vartheta,\varphi) = \frac{N_0}{2}\left[1 + \left(a_0 \pm A_y(\vartheta,T_{\rm p})P_x^{\rm fp}\right)\cos\varphi + \left(b_0 \mp A_y(\vartheta,T_{\rm p})P_y^{\rm fp}\right)\sin\varphi\right] ,$$

where $N^{\pm}(\vartheta,\varphi)$ is the number of protons hit by an incoming electron of helicity state ($\pm$) and scattering in the FPP at angles (ϑ, φ), N_0 is the number of incoming protons in the FPP, $A_y(\vartheta,T_{\rm p})$ is the analyzing power of the graphite analyzer, and a_0 and b_0 are false asymmetries, induced by possible misalignment of the chambers and straw inefficiencies. The $P_x^{\rm fp}$ and $P_y^{\rm fp}$ are the two proton polarization components perpendicular to the momentum. Here, the $\hat{z}$-axis is defined along the particle momentum, the $\hat{x}$-axis is along the momentum dispersion direction, and $\hat{y} = \hat{z} \times \hat{x}$.

The helicity-dependent polarization transfered to the proton from the electron beam can be obtained by taking the difference between the two distributions for the + and − helicity states:

$$N^{\rm diff} = \frac{N_0}{2}A_y(\vartheta,T_{\rm p})\left(P_x^{\rm fp}\cos\varphi - P_y^{\rm fp}\sin\varphi\right) .$$

Note that the false asymmetries have disappeared, because we measure the transfered polarization. The helicity-independent, induced polarization is obtained by summing the two helicity state contributions:

$$N^{\rm sum} = \frac{N_0}{2}\left[1 + \left(a_0 + A_y(\vartheta,T_{\rm p})P_x^{\rm fp}\right)\cos\varphi + \left(b_0 - A_y(\vartheta,T_{\rm p})P_y^{\rm fp}\right)\sin\varphi\right] .$$

In this case, the false asymmetries must be determined by using unpolarized scattering off a hydrogen target, for which no asymmetry should arise (except for possible instrumental ones).

The analyzing-power angular distributions at a given kinetic energy are well known, from calibration data from Saclay, Jefferson Lab, and others. Note that we can also easily calibrate the analyzing powers for our momentum settings using elastic scattering of polarized electrons off a proton target.

The FPP measures the polarization of the proton at the focal plane of the spectrometer. To extract the three components P'_x, P'_z and P_y, we need to transport this polarization back to the target and take into account the precession of the spin through the magnetic fields. In a perfect dipole approximation, the precession matrix is given by:

$$P_x^{\rm fp} = -P'_z\sin\chi + P_y\cos\chi \quad (9)$$

$$P_y^{\rm fp} = P'_x \quad (10)$$

The precession angle χ is given by

$$\chi = (\mu_{\rm p} - 1)\gamma\,\Theta_{\rm bend} ,$$

where $\mu_{\rm p}$ is the magnetic moment of the proton, γ is the relativistic boost and $\Theta_{\rm bend}$ is the total bending angle inside the spectrometer.

In reality, we have to take into account event by event deviations from this perfect dipole approximation. The precession matrix becomes

$$\begin{pmatrix} P_x^{\rm fp} \\ P_y^{\rm fp} \\ P_z^{\rm fp} \end{pmatrix} = \begin{pmatrix} S_{xx} & S_{xy} & S_{xz} \\ S_{yx} & S_{yy} & S_{yz} \\ S_{zx} & S_{zy} & S_{zz} \end{pmatrix} \begin{pmatrix} P'_x \\ P_y \\ P'_z \end{pmatrix} .$$

The coefficients S_{ij} are calculated using the external code COSY, and the polarization components at the target are extracted using a maximum-likelihood method. This analysis method has been extensively used for this polarimeter. In polarization measurements, the main source of systematic error lies in the uncertainty in the precession of the polarization. Careful alignment studies of the HRS magnetic elements have been performed [48], and the precession code COSY has been optimized so that eventually, the total uncertainty of the measurement is mostly dominated by the statistics (see below for details).

The statistical uncertainties on the asymmetries measured in the FPP, thus on the polarization components, are given by

$$\Delta P_x^{\rm fp} = \Delta P_y^{\rm fp} = \sqrt{\frac{2}{N_0 f}} .$$

Here f is the figure of merit of the polarimeter, given by

$$f = \int_{\vartheta_{\rm min}}^{\vartheta_{\rm max}} \epsilon(\vartheta) A_y^2(\vartheta) d\vartheta ,$$

where $\epsilon(\vartheta)$ is the efficiency of the polarimeter at a given scattering angle. Translated to target quantities, the error becomes, according to Eqs. (9-10):

$$\Delta P'_x = \frac{1}{P_{\rm e}} \sqrt{\frac{2}{N_0 f}} , \tag{11}$$

$$\Delta P_y = \frac{1}{\cos\chi} \sqrt{\frac{2}{N_0 f}} , \tag{12}$$

$$\Delta P'_z = \frac{1}{P_{\rm e}} \frac{1}{\sin\chi} \sqrt{\frac{2}{N_0 f}} . \tag{13}$$

Table 2 lists the spin-precession angles and figures of merit for each kinematics. We have excellent figures of merit and favourable spin-precession angle to the FPP to allow good measurements of all three polarization components.

5.2 FPP systematic uncertainties

As focal-plane polarimetry involves ratios of polarized and polarized parts of the cross-section, many systematic errors are suppressed. The remaining uncertainties linked to

Table 2 — Simulated FPP parameters for different kinematics: spin-precession angle χ and the figure of merit f.

E_e [MeV]	Q^2 [(GeV/c)^2]	W [MeV]	χ [°]	f
2000	0.13	1440	118.7	0.0166
3000	0.33	1440	130.0	0.0125
3000	0.53	1440	140.7	0.0112
3000	0.73	1440	151.0	0.0102
3000	0.93	1440	161.1	0.0100
2000	0.13	1380	112.5	0.0166
2000	0.13	1410	115.5	0.0166
2000	0.13	1440	118.7	0.0166
2000	0.13	1470	121.9	0.0150
2000	0.13	1500	125.3	0.0150
3000	0.33	1380	123.7	0.0150
3000	0.33	1410	126.8	0.0125
3000	0.33	1440	130.0	0.0125
3000	0.33	1470	133.2	0.0125
3000	0.33	1500	136.6	0.0120

the polarimeter are small compared to the statistical uncertainties. First, some error may arise from uncertainties in the scattering angle in the FPP. A 1 mrad precision in the determination of this angle leads to uncertainties of the order of 1 % in the polarization. The second source of systematic uncertainties is the treatment of the precession inside the spectrometer. Careful studies of the alignment of the magnetic elements have reduced the associated error to the percent level [48]. Also, for the transferred part of the polarization, the uncertainty of the beam polarization must be taken into account. The beam polarization will be measured continuously with the Hall A Compton polarimeter, with the combined statistical and systematic errors on the order of 1.3 % (values determined in E91-011 [49]). The overall systematic error of the polarization measurement is anticipated to be below 3 %.

5.3 Requirements on other experimental equipment

The measurements will be performed by using two High Resolution Spectrometers (HRSs) of Hall A. One of them will be used in the standard detector configuration for detection of electrons, while the other will be equipped with the existing focal-plane polarimeter to measure the polarization of recoil protons. Beam currents of 75 μA, with an anticipated degree of polarization of $\sim$ 75 % are required. The 15 cm LH2 cryo-target will be used. All these requirements can be met with the standard equipment of Hall A.

6 Count-rate estimates and beam-time request

We have used the most recent version of the MAID model [43] to compute the cross-sections and the Hall A Monte-Carlo package MCEEP to simulate the experimental phase space. This combination worked well previously and the count rates were seen to match those actually observed in the E91-011 experiment [37]. Beam currents of 75 μA impinging on a 15 cm LH2 cryo-target will be used, yielding a luminosity of $\sim 2\cdot10^{38}/\mathrm{cm}^2\mathrm{s}$. The single count rates were estimated with the computer codes EPC and QFSV of Lightbody and O'Connell [50] and are listed in Table 3.

Table 3 — Estimates of singles, accidental, and true coincident rates for the proposed kinematics, with a beam current of $I_e = 75\,\mu$A.

					—— Singles ——			Accid.	Trues
E_e	Q^2	W	θ_e	θ_p	(e)	(p)	(π^+)	(ep)	(ep)
[MeV]	[(GeV/c)^2]	[MeV]	[°]	[°]	[kHz]	[kHz]	[kHz]	[Hz]	[Hz]
2000	0.13	1440	12.9	21.3	398	117	223	10	17
3000	0.33	1440	12.9	29.4	380	79	86	2.3	12
3000	0.53	1440	16.8	30.8	115	41	34	0.37	5
3000	0.73	1440	20.2	30.8	46	23	16	0.09	2
3000	0.93	1440	23.5	30.1	21	14	9	0.03	1
2000	0.13	1380	12.4	24.7	411	119	221	11	20
2000	0.13	1410	12.6	23.0	382	118	221	10	17
2000	0.13	1440	12.9	21.3	398	117	223	10	17
2000	0.13	1470	13.1	19.8	457	115	223	12	16
2000	0.13	1500	13.4	18.5	451	111	219	12	25
3000	0.33	1380	12.6	32.7	335	79	82	2	18
3000	0.33	1410	12.7	31.0	348	79	84	2	13
3000	0.33	1440	12.9	29.4	380	79	86	2	12
3000	0.33	1470	13.0	27.8	423	80	90	3	13
3000	0.33	1500	13.2	26.4	411	79	92	3	16

For kinematics at fixed $Q^2 = 0.13$ and 0.33 (GeV/c)^2 (the "W-scans"), a single setting of the electron spectrometer could cover practically the complete W-range. However, due to acceptance fall-off, and in order to avoid excessive problems in averaging over the acceptance, it is better to acquire data in individual energy settings and take only the corresponding central (30 MeV wide) bin in W. In the "Q^2-scans", the range in W was restricted to $W = (1440 \pm 15)$ MeV. In all settings, parallel kinematics was enforced in the simulation by a $\theta^\star_{pq} \leq 10^\circ$ cut.

Table 4 gives the coincidence count-rate estimates, the absolute statistical uncertainties on the recoil polarization components, and the beam-time request.

Table 4 — The coincidence rates, absolute statistical uncertainties on the recoil polarization components, and the beam-time request with $I_e = 75\,\mu$A.

E_e	Q^2	W	(e, e′p)	$\Delta(P'_x/P_e)$	ΔP_y	$\Delta(P'_z/P_e)$	Beam time [h]
2000	0.13	1440	17	0.0110	0.0229	0.0126	16
3000	0.33	1440	12	0.0156	0.0243	0.0204	15
3000	0.53	1440	5	0.0189	0.0245	0.0298	27
3000	0.73	1440	2	0.0210	0.0240	0.0432	55
3000	0.93	1440	1	0.0230	0.0243	0.0710	89
2000	0.13	1380	20	0.0091	0.0237	0.0098	20
2000	0.13	1410	17	0.0103	0.0239	0.0114	19
2000	0.13	1440	17	0.0110	0.0229	0.0126	–
2000	0.13	1470	16	0.0125	0.0236	0.0147	15
2000	0.13	1500	25	0.0137	0.0237	0.0168	8
3000	0.33	1380	18	0.0161	0.0291	0.0194	8
3000	0.33	1410	13	0.0171	0.0286	0.0214	12
3000	0.33	1440	12	0.0156	0.0243	0.0204	–
3000	0.33	1470	13	0.0198	0.0289	0.0271	9
3000	0.33	1500	16	0.0206	0.0284	0.0301	7
		FPP calibration					24
		2×Møller					16
		2×Beam energy					8
		Total					348

6.1 The “double-FPP” option

In the RCS experiment E99-114 [51], an extension of the focal-plane polarimeter apparatus was utilized. In addition to the carbon analyzers between the front and rear straw chambers, additional CH_2-analyzer material was inserted between the VDC package and the front straw chambers. The setup can then be operated as a double focal-plane polarimeter since the particle tracks between pairs of tracking planes are measured to great precision. This doubled the efficiency at no cost in analyzing power.

We are presently exploring the possibility of using the additional analyzer in our experiment. Even if the analyzing power of the additional analyzer turned out to be relatively small, the overall figure-of-merit in such a “double-FPP” setup would still be greater

or equal to the one in the case of a single carbon analyzer. Due to this uncertainty, which can only have a better outcome, the present count-rate calculations and the corresponding beam-time requests shown in the Tables and Figures were made without the additional analyzer.

6.2 Systematic uncertainties

The two beam energies used in our experiment will be measured to a relative accuracy better than 10^{-3}, implying a $\lesssim 2\,\mathrm{MeV}$ uncertainty in E_e.

The spectrometers will be positioned at small angles, at less than $\sim 20^\circ$ for the electron arm, and less than $\sim 30^\circ$ for the proton arm for most of the kinematic settings. At such small angles, the quality of the vertex determination both along the beam (z or $y_0 = z\sin\theta_\mathrm{e}$) and in the transverse direction deteriorate slightly, but even at the extreme HRS angle of 12.5°, δz does not exceed 6 mm FWHM. The uncertainty in vertex position implies an uncertainty in the energy losses of the emerging electrons and protons. For electrons it amounts to less than $\delta E'_\mathrm{e} \lesssim 1.5\,\mathrm{MeV}$, while for the least energetic protons in our kinematics, this corresponds to $\delta T_\mathrm{p} \lesssim 1\,\mathrm{MeV}$. The δE_e and $\delta E'_\mathrm{e}$ have an influence on the overall uncertainty in W, but it is an order of magnitude smaller than the bin-size of 30 MeV used in both Q^2- and W-scans.

Multiple scattering for electrons in the LH_2 target is below 1 mrad, so the achievable energy resolutions described above and the precision of the θ_e measurement are more than sufficient for the proposed binning in Q^2.

For protons, multiple-scattering angles are below 2 mrad, which introduce a negligible systematic uncertainty in the reconstruction of the proton spin precession through the spectrometer. Typically, ~ 1 mrad uncertainties in the secondary (FPP) scattering angles translate into a relative uncertainty on the polarization components at a one-percent level. The uncertainty in the spin precession is predominantly of systematic origin as it involves a model (COSY). The uncertainties drop for P_y and increase for P'_z when the precession angle χ approaches 180° (see Eqs. (12) and (13)), but the effects are small for our range of proton momenta. For a more detailed discussion of the combined statistical and systematic uncertainties of the polarization measurements (focal-plane polarimeter and electron-beam polarimetry), please refer to Subsection 5.2. The overall systematic error of the polarization measurement is anticipated to be below 3 %, and is dominated by the uncertainty of the COSY model.

7 Summary

The Roper resonance is the lowest positive-parity $N^\star$ state and is of paramount theoretical and experimental significance. Yet, it has been relatively scantly studied experimentally, in particular with respect to the more familiar Δ resonance. Very little is known about the multipole structure of the $N \rightarrow R$ transition in single-pion electroproduction. An almost complete lack of data from polarized experiments is partly responsible for this disparity.

Models indicate that the sensitivities of particular double-polarization observables in both photo- and electro-production to the Roper are tremendous (G and P'_x, P_y, respectively), and that the separation of resonant and background contributions is not problematic and has very little model dependence. An outstanding theoretical issue is to improve the quality of the partial-wave analyses, but more precision electro-production data, especially of double-polarized observables, are needed in order to stabilize the fits.

We propose to study the structure of the Roper resonance by measuring the recoil proton polarization components P'_x, P_y, and P'_z in the $p(\vec{e}, e'\vec{p})\pi^0$ reaction. These components exhibit strong sensitivities to the pertinent Roper multipoles M_{1-} and S_{1-}, and will be measured in a broad range of Q^2 and W. It is this extended coverage that will provide a fruitful and instructive study of the transition through comparison with the state-of-the-art models, which are just beginning to evolve beyond the first resonance region. It will provide severe constraints on these models in a domain where only scarce cross-section and double-polarization data exist.

References

[1] L. D. Roper, Phys. Rev. Lett. **12** (1964) 340.

[2] D. M. Manley, E. M. Saleski, Phys. Rev. D **45** (1992) 4002.

[3] R. E. Cutkosky, C. P. Forsyth, R. E. Hendrick, R. L. Kelly, Phys. Rev. D **20** (1979) 2839.

[4] S. Eidelman et al. (Particle Data Group), Phys. Lett. B **592** (2004) 1.

[5] Z. Li, Phys. Rev. D **44** (1991) 2841.

[6] Z. Li, V. Burkert, Z. Li, Phys. Rev. D **46** (1992) 70.

[7] C. Gerhardt, Z. Phys. C **4** (1980) 311.

[8] B. Boden, G. Krösen, Research Program at CEBAF, Report of the 1986 Summer Study Group, V. Burkert (ed.), p. 121.

[9] L. S. Kisslinger, Z. Li, Phys. Rev. D **51** (1995) R5986.

[10] C. E. Carlson, N. C. Mukhopadhyay, Phys. Rev. Lett. **67** (1991) 3745.

[11] S. Capstick, P. R. Page, Phys. Rev. D **60** (1999) 111501.

[12] G. L. Strobel, K. V. Shitikova, Phys. Rev. C **56** (1997) 551.

[13] G. L. Strobel, Int. J. Theor. Phys. **39** (2000) 115.

[14] N. Mathur et al., arXiv:hep-ph/0306199.

[15] Y. Chen et al., arXiv:hep-ph/0306199.

[16] D. Guadagnoli, M. Papinutto, S. Simula, arXiv:hep-lat/0409011.

[17] Fl. Stancu, P. Stassart, Phys. Rev. D **41** (1990) 916.

[18] Z. Li, F. E. Close, Phys. Rev. D **42** (1990) 2207.

[19] S. Capstick, Phys. Rev. D **46** (1992) 1965.

[20] S. Capstick, Phys. Rev. D **46** (1992) 2864.

[21] H. J. Weber, Phys. Rev. C **41** (1990) 2783.

[22] S. Capstick, B. D. Keister, Phys. Rev. D **51** (1995) 3598.

[23] F. Cardarelli, E. Pace, G. Salmè, S. Simula, Phys. Lett. B **397** (1997) 13.

[24] F. Cano, P. González, Phys. Lett. B **431** (1998) 270.

[25] U. Meyer, A. J. Buchmann, A. Faessler, Phys. Lett. B **408** (1997) 19.

[26] Y. B. Dong, K. Shimizu, A. Faessler, A. J. Buchmann, Phys. Rev. C **60** (1999) 035203.

[27] P. Alberto, M. Fiolhais, B. Golli, J. Marques, Phys. Lett. B **523** (2001) 273.

[28] Th. Meissner, F. Grümmer, K. Goeke, M. Harvey, Phys. Rev. D **39** (1989) 1903.

[29] K. Bermuth, D. Drechsel, L. Tiator, J. B. Seaborn, Phys. Rev. D **37** (1988) 89.

[30] B. C. Pearce, I. R. Afnan, Phys. Rev. C **40** (1989) 220.

[31] J. A. Elsey, I. R. Afnan, Phys. Rev. C **40** (1989) 2353.

[32] K. Joo et al. (CLAS Collaboration), Phys. Rev. C **68** (2003) 032201(R).

[33] K. Joo et al. (CLAS Collaboration), Phys. Rev. C **70** (2004) 042201(R).

[34] I. G. Aznauryan et al., arXiv:nucl-th/0407021, to be published in Phys. Rev. C.

[35] L. Tiator et al., Eur. Phys. J. A **19** (2004) 55.

[36] N. Benmouna, G. O'Rielly, I. Strakovski, S. Strauch, JLab Experiment E03-105.

[37] J. J. Kelly, A. Sarty, S. Frullani (co-spokespersons), JLab Experiment E91-011.

[38] Th. Pospischil et al. (A1 Collaboration), Phys. Rev. Lett. **86** (2001) 2959.

[39] D. Drechsel, O. Hanstein, S.S. Kamalov, L. Tiator, Nucl. Phys. **A** 645 (1999) 145.

[40] S. S. Kamalov, S. N. Yang, Phys. Rev. Lett. **83** (1999) 4494.

[41] S. S. Kamalov et al., Phys. Rev. C **64** (2001) 032201(R).

[42] T. Sato, T.-S.H. Lee, Phys. Rev. C **63** (2001) 055201.

[43] http://www.kph.uni-mainz.de/MAID/maid2003/maid2003.html

[44] http://www.kph.uni-mainz.de/MAID/dmt/dmt2001.html

[45] T. Sato, private communication (2004).

[46] L. Tiator, contribution to NSTAR 2004 (in preparation), and private communication (2004).

[47] A. Picklesimer, J. W. van Orden, Phys. Rev. C **35** (1987) 266.

[48] L. Pentchev, J. J. LeRose, JLab-TN-01-052 (2001).

[49] S. Escoffier, PhD Thesis (2001); see also JLab-TN-01-052 (2001).

[50] J. Lightbody, J. S. O'Connell, Computers in Physics **2** (1988) 57.

[51] C. Hyde-Wright, A. Nathan (co-spokespersons), JLab Experiment E99-114.